

Quantifying Exciton Annihilation Effects in Thermally Activated Delayed Fluorescence Materials

Kalyani Thakur, Bas van der Zee, Gert-Jan A. H. Wetzelaer, Charusheela Ramanan, and Paul W. M. Blom*

Important parameters for the design and performance of thermally activated delayed fluorescence (TADF) emitters are the forward and reverse intersystem crossing rates between singlet and triplet states. The magnitude of these rates is determined from the prompt and delayed transient photoluminescence decay. It is demonstrated that this photoluminescence decay strongly depends on the initial photoexcited population density due to exciton–exciton annihilation processes. By kinetic modeling of the power-dependent time-resolved photoluminescence of the TADF emitter 9,10-bis(4-(9H-carbazol-9-yl)-2,6-dimethylphenyl)-9,10-diboraanthracene (CzDBA), singlet–triplet annihilation and triplet–triplet annihilation are identified as the main loss processes with rate constants in the order of $10^{-17} \text{ m}^3 \text{ s}^{-1}$. Neglecting these quenching processes leads to erroneous estimates of the (reverse) intersystem crossing rates.

1. Introduction

Thermally activated delayed fluorescence (TADF) materials are an emerging class of molecular systems utilized in the third generation of organic light-emitting diodes (OLEDs), which are showing great promise for highly efficient OLEDs in future commercial applications^[1–3] as well as in other fields, such as bioimaging.^[4–6] These molecules offer the possibility to harvest light from both singlet and triplet excitons, allowing for a potential 100% internal quantum efficiency (IQE) in OLEDs. In contrast to earlier generation phosphorescent emitters, TADF systems can harvest triplet excitons without the incorporation of heavy metals in their molecular structure.^[3] The molecular structure of TADF emitters consists of electron donor and electron acceptor moieties with strong through-bond or through-

space charge transfer coupling. This leads to a very small energy gap between the singlet charge-transfer (S_1) and triplet charge-transfer (T_1) states (usually only several tens of meV). As a result, excitons in the dark T_1 state undergo reverse intersystem crossing (rISC) at room temperature to the emissive S_1 state, contributing as delayed fluorescence (DF) to the light output next to the regular prompt fluorescence (PF) (Figure 1).^[7]

The simplified Jablonski diagram in Figure 1a depicts the electronic transitions in a TADF system. After generating excitons with singlet and triplet character, singlet excitons relax to the ground state on a timescale of nanoseconds, termed prompt fluorescence (PF). Triplet excitons can undergo rISC, resulting in delayed

fluorescence from S_1 on the timescale of microseconds. The overall fluorescence efficiency of a TADF material depends on the rates of forward (k_{ISC}) and reverse (k_{rISC}) intersystem crossing between S_1 and T_1 . These photophysical parameters are typically characterized using time-resolved photoluminescence measurements (TRPL) to track the dynamic evolution of the S_1 emission. A typical TRPL curve for a TADF system exhibits a bi-modal decay, attributed to the PF and DF contributions to the PL. This is often described by using a biexponential function^[8–10]

$$I(t) = A_1 \exp\left(-\frac{t}{\tau_{\text{PF}}}\right) + A_2 \exp\left(-\frac{t}{\tau_{\text{DF}}}\right) \quad (1)$$

Photophysical parameters such as the singlet lifetime τ_s and triplet lifetime τ_t are then derived and used to calculate the intersystem crossing (ISC) rate k_{ISC} and rISC rate k_{rISC} , along with the prompt/delayed fluorescence quantum yields ($\varphi_{\text{PF}}/\varphi_{\text{DF}}$). The k_{rISC} is then given by^[11]

$$k_{\text{rISC}} = \frac{1}{\tau_{\text{DF}}} \frac{\varphi_{\text{PF}} + \varphi_{\text{DF}}}{\varphi_{\text{PF}}} \quad (2)$$

However, the bi-exponential model relies on several assumptions that are not always valid. First, the relationships only hold when $\varphi_{\text{DF}} \geq 4 \times \varphi_{\text{PF}}$, requiring that the quantum yield of fluorescence via the triplet state be more than four times the yield obtained directly from singlet decay.^[12,13] This assumption makes sure that the rISC is close to 100% in the material.

K. Thakur, B. van der Zee, G.-J. A. H. Wetzelaer, C. Ramanan, P. W. M. Blom
Max Planck Institute for Polymer Research
Ackermannweg 10, 55128 Mainz, Germany
E-mail: blom@mpip-mainz.mpg.de

 The ORCID identification number(s) for the author(s) of this article can be found under <https://doi.org/10.1002/adom.202101784>.

© 2021 The Authors. Advanced Optical Materials published by Wiley-VCH GmbH. This is an open access article under the terms of the Creative Commons Attribution-NonCommercial-NoDerivs License, which permits use and distribution in any medium, provided the original work is properly cited, the use is non-commercial and no modifications or adaptations are made.

DOI: 10.1002/adom.202101784

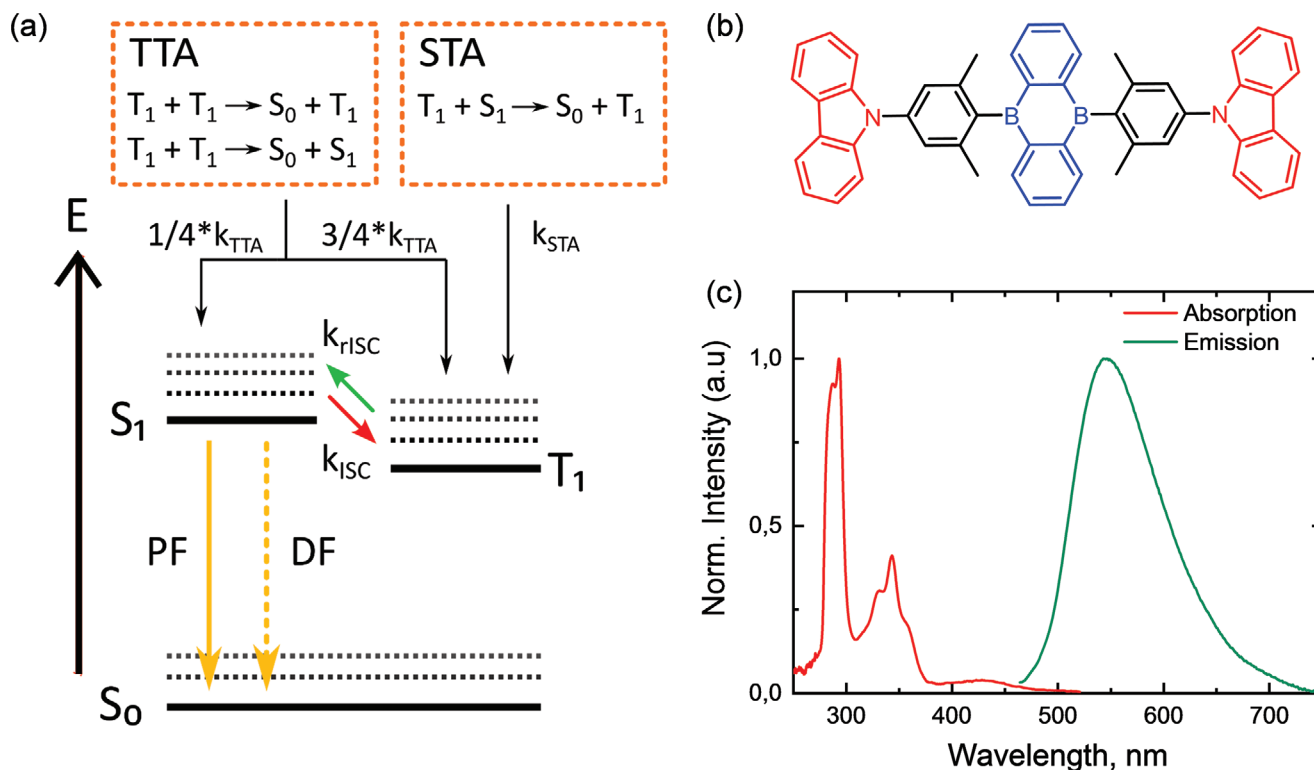


Figure 1. a) Mechanism of TTA and STA processes (top) and their relative contributions under electrical excitation (black arrows) to the excited state energy levels of a TADF material, which are depicted in the Jablonski diagram below. The working mechanism of a TADF material relies on efficient forward and reverse intersystem crossing (ISC and rISC) between the excited singlet and triplet charge-transfer states (S_1 and T_1). b) Molecular structure of CzDBA, which consists of two donor carbazole units (red) connected to the diboraanthracene acceptor (blue). c) The steady-state absorption (red) and emission (green) spectra of CzDBA in toluene.

Furthermore, for TADF systems in the solid state, a multiexponential PL decay may be observed. A common practice has been to use multiexponential fitting with three to four components. In order to still obtain a characteristic time constant for the PF and DF the fast components are then averaged and assigned to PF, whereas the time average of the slow components is then taken as representative for DF. The occurrence of multiple time constants has been attributed to the conformational distribution of the molecules in the solid-state film and incomplete geometrical relaxation of the excited states. We note that this behavior is similar to observations in polymer semiconductors, which exhibit heterogeneous photoexcited lifetimes due to energy transfer, conformational disorder, and spectral diffusion in the solid state.^{[14],[15]} In OLEDs, TADF emitters are typically diluted in a wide bandgap host. When diluting an emitter, a variety of local environments introduces several molecular conformations, which can lead to a spread in CT energies and thus rISC rates, justifying the use of a multiexponential fit.^[16] But in the case of a neat film of the TADF emitter 9,10-bis(4-(9H-carbazol-9-yl)-2,6-dimethylphenyl)-9,10-diboraanthracene (CzDBA), the PL decay was fitted with a three exponential model, and τ_{DF} was then taken as the average of the two slow components.^[17] Since the physical origin of a third decay component is not clear, such an approach might lead to a misinterpretation of the DF decay time τ_{DF} and therefore to erroneous estimates of the forward (k_{ISC}) and reverse (k_{rISC}) intersystem crossing rates.

Another limitation of the model described in Equation (1) is that it does not account for additional excited state deactivation pathways, especially nonradiative recombination including various annihilation processes. Such quenching processes play an important role in the device performance of TADF OLEDs and efficiency roll-off at high luminance.^[18–21] These include triplet-triplet annihilation (TTA), triplet-polaron quenching (TPQ), and singlet-triplet annihilation (STA). For the emitter 1,2,3,5-tetrakis(carbazol-9-yl)-4,6-dicyanobenzene (4CzIPN) it was shown that the PL quantum yield below 100 K is strongly suppressed and accompanied by a strong dependence of the transient PL on excitation intensity, which was attributed to the occurrence of a TTA process.^[19] Figure 1a describes how these processes can affect the fluorescence output of a TADF system. In TTA two triplet excitons interact to form an intermediate state, which finally decays into a singlet or triplet, lowering the overall number of the total emissive excitons. Note that we here omit the formation of the quintet state, although allowed by conservation of total momentum, since its energy lies too high to be reached at room temperature.^[20] Similarly in STA, one singlet and triplet interact together where the singlet decays nonradiatively to the ground state, and only the triplet excited state remains. These nonradiative pathways are highly dependent on experimental conditions, such as excitation density, and can affect the reproducibility of the PL decay. This in turn influences the interpretation of photophysical dynamics in TADF systems.

As an alternative for the biexponential model, kinetic rate models have been used to fit PL transients based on measurable inputs and subsequently extract photophysical parameters, including contributions from annihilation.^[22–24] Annihilation processes depend on the incident laser power in PL experiments and thus a systematic investigation into these quenching processes can therefore be conducted by studying the power dependence of the prompt and delayed fluorescence. In earlier work, power-dependent PL curves were fitted with rate equations incorporating various quenching processes.^[23] However, this analysis led to power-dependent annihilation constants, which showed no clear correlation with their respective power density. In this paper, we combine power-dependent time-resolved PL measurements with a kinetic modelling approach based on rate equations of the singlet and triplet exciton concentrations using CzDBA as efficient model system. This method can be universally applied to all TADF emitters, irrespective of their PF/DF yield. Our results show that the power-dependent PL decays can be fit correctly by incorporating TTA and STA and STA, leading to quenching constants in the order of $\approx 10^{-17} \text{ m}^3 \text{ s}^{-1}$. The quantified quenching constants further allow us to calculate the relative contribution of the various loss processes to the overall loss of singlet excitons as a function of time and excitation power density. This approach can be generally utilized for all TADF materials to provide more reliable and accurate characterization of their photophysical rate constants.

2. Results and Discussion

2.1. CzDBA Film PL Decay Exhibits Contributions from Annihilation Mechanisms

The TADF emitter CzDBA was chosen as a model system to characterize the PL decay. This material exhibits high PLQY in neat films (>90%), low trap/defect density, low self-quenching,^[17,25] and has been utilized in a high-performance undoped single-layer OLED with EQE values of 19%.^[25] The steady-state absorption and fluorescence spectra of the CzDBA solution are shown in Figure 1c and are consistent with the spectra reported in literature.^[17] The absorption peaks are located at 293 nm (Cz donor), 343 nm (DBA acceptor), and a small tail centered at 430 nm arising from the intramolecular

charge-transfer (CT) state absorption. CzDBA exhibits a broad featureless fluorescence spectrum with its maximum at 544 nm, characteristic of emission from a CT state, as is typical for TADF materials.^[17,26]

We measured the PL decay dynamics of CzDBA in solution and in film to disentangle intrinsic versus multichromophoric contributions, as shown in Figure 2. The films are photoexcited at 350 nm and the TRPL kinetics are averaged across the 542–545 nm wavelength range. While all of the decay curves qualitatively exhibit a bimodal line shape that is expected for a TADF emitter, we find that the PL transient of the solid film cannot be well described using the simple biexponential function given by Equation (1).

The PL decay kinetics of CzDBA in solution are well fit using a biexponential function. We assume no multichromophore processes in the solution measurement, and so the physical significance of this biexponential fit is explained as a linear combination of prompt and delayed fluorescence mechanisms (τ_{PF} and τ_{DF}). In this case, the prompt fluorescence (τ_{PF}) is attributed to the singlet lifetime and represents the decay to the ground state S_0 of excitons that initially populate S_1 . The delayed fluorescence (τ_{DF}) arises from fluorescence that occurs as a result of the repopulation of S_1 by T_1 via rISC, and is therefore correlated to the effective triplet lifetime. Therefore, $\tau_{\text{PF}} = \tau_s$ and $\tau_{\text{DF}} = \tau_t$. Based on this, we retrieve values of $\tau_s = 100 \text{ ns}$ and $\tau_t = 1.8 \mu\text{s}$ for CzDBA in solution. This is in agreement with previously reported values.^[26] Note that the effective triplet lifetime is the time an exciton remains in the triplet state and is not to be confused with the intrinsic triplet lifetime, which would represent the decay of the triplet to the ground state (phosphorescence). Intrinsic triplet lifetimes are commonly in the order of 100 μs to even ms,^[27,28] but in the case of TADF systems, rISC presents a faster deactivation pathway for the triplet state.

The TRPL measurement was also carried out on a CzDBA neat film, measured at four different excitation power densities (Figure S1, Supporting Information). The shape of the decay curves depends on the excitation power, with the film exhibiting a faster decay lifetime with increasing excitation power. The decay curves for the lowest and highest excitation powers are shown in Figure 2b, along with attempted biexponential fits using Equation (1). In contrast to CzDBA in solution, the biexponential fit strongly deviates from the measured PL decay for the neat film. This effect is particularly pronounced in the

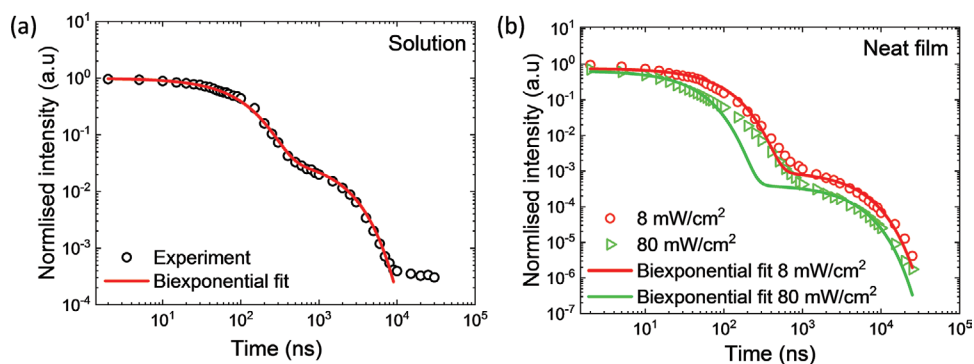


Figure 2. a) The PL transient of CzDBA in solution at a power density of 8 mW cm^{-2} in black with its biexponential fit in red. b) The PL transient of a CzDBA neat film at power densities of 8 mW cm^{-2} (red) and 80 mW cm^{-2} (green) where the solid lines represent their biexponential fit, respectively.

intermediate time scale (100–1000 ns). The deviation is also greater at the higher 80 mW cm⁻² excitation power than at the lower 8 mW cm⁻² excitation power. This suggests that the origin of the deviation depends on the initial photoexcited population.

We further note that the PL decay in film exhibits a longer lifetime than that in solution, ≈4.0 versus 1.8 μs. This is attributed to conformational freedom in solution leading to enhanced vibronic coupling and therefore increased nonradiative internal conversion to the ground state. This finding is supported by the high PLQY value of >90% in neat CzDBA films versus only 14% in solution.^[17] Despite this evidence for decreased nonradiative quenching due to internal conversion in the film samples, the lack of agreement with a biexponential fit and the observed power dependence indicates that other nonradiative quenching mechanisms arise in the neat film, which are not present in solution.

The results shown in Figure 2b clearly show that at a high excitation power density (80 mW cm⁻²) the biexponential decay model cannot describe the CzDBA PL decay dynamics in the solid-state. Previous work on TADF systems has also reported such observations.^[13,16,29] Even at lower excitation density (8 mW cm⁻²) there is still some discrepancy between the model and experiment. Applying the biexponential model to this lower intensity (red solid line) would result in τ_s and τ_i of 75 ns and 4.0 μs, respectively. Similarly, for higher excitation density (80 mW cm⁻²) τ_s and τ_i would be 33 ns and 3.5 μs, respectively, which clearly indicates the power dependence of prompt and delayed lifetimes.

2.2. Kinetic Modeling Deconvolutes Exciton Annihilation Contributions to PL Decay

An alternative approach to analyze the PL decay that also incorporates quenching processes is to model the transient PL using rate equations for the singlet and triplet exciton populations.

It is known that in PL measurements the emission occurs predominantly from the charge transfer state (CT), but the operation of a TADF system involves locally excited singlet and triplet states as well.^[30] After photoexcitation, a singlet can also first be generated in the locally excited singlet (LE) state which can decay radiatively before undergoing electron transfer to form a CT state. It is the singlet CT state that is being continuously repopulated through rISC, not the LE state, meaning that only at early times in a PL decay LE states could potentially play a role. Similarly, the rISC does not directly occur from the triplet CT state but it first undergoes vibronic mixing between locally excited triplet states and CT state and proceed via LE to the singlet CT state.^[31] The time scale at which the mixing takes place is very fast compared to the observed prompt and delayed lifetime. The contribution of the LE singlet state to the total light output is low, whereas the LE and CT triplet state can be effectively considered as one.^[22] The same holds for higher lying triplet states. Quantum chemical calculations (details in the Experimental Section) of excited state energy levels in the solid state environment reveal that T₁ and T₂ lie at 2.471 and 2.504 eV, respectively. These excited triplet states are almost degenerate in energy and thus act effectively as one energy level. Furthermore, the T₃ state is located at 2.886 eV and is a

local excitation, which therefore does not play a role in the rISC process. Hence, the TADF dynamics can be approximated by a three energy level model, considering only S₀, S₁, and T₁ and the interactions between them as described in Figure 1a. Note that the absence of charge carriers in PL measurements means that the aforementioned TPQ mechanism will not play a role, and is therefore neglected.

Correspondingly, the rate equation for the singlet density [S] and triplet density [T] for a three-level model is given by

$$\frac{d[S]}{dt} = [S_0] - \frac{[S]}{\tau_s} - k_{ISC}[S] + k_{rISC}[T] - k_{SSA}[S][S] - k_{STA}[S][T] + 0.25k_{TTA}[T][T] \quad (3)$$

$$\frac{d[T]}{dt} = -\frac{[T]}{\tau_T} + k_{ISC}[S] - k_{rISC}[T] - 1.25k_{TTA}[T][T] \quad (4)$$

where [S₀] is the initial singlet density, k_{SSA} is the singlet–singlet annihilation constant, k_{STA} is the singlet–triplet annihilation constant, k_{TTA} is the triplet–triplet annihilation constant, [S] is the singlet concentration, and [T] is the triplet concentration. To exclude the contribution of specific quenching processes, their respective annihilation coefficient can simply be set to zero. Equations (3) and (4) are solved in a numerical fashion using the finite difference method with a sufficiently small time step of 5 ns. The various rate constants can subsequently be extracted from fitting the normalized PL data to [S].

Figure 3 shows the kinetic modeling of film PL kinetics at power densities of 8 and 80 mW cm⁻², considering no annihilation a), each STA b), and TTA c) independently, and finally STA and TTA together d). In Figure 3a, the PL decays are modeled assuming no contribution from TTA or STA quenching processes. In that case, the fitting for the two power densities is on top of each other and fails to reproduce the experiment in both the PF and DF part and their power dependence. We attempted to improve the fit using a reduced singlet lifetime of 65 ns as well (Figure S2, Supporting Information). However, the fit still does not match the experimental data in the transition region between the time scale of 10–1000 ns, and the higher power density cannot be fit at all (not shown). This strongly supports our hypothesis that TTA and STA quenching phenomena are playing a crucial role in these film decay dynamics.

Next, we modeled the PL decays with an included contribution from STA (Figure 3b). This model describes the prompt emission very well. However, the fit insufficiently describes the delayed emission. Similarly, we attempted to fit the data considering only quenching by TTA (Figure 3c). In this case, the model successfully fits the delayed emission at later times and improves the fit of the transition region between PF and DF at higher powers, but fails to describe the faster prompt fluorescence region. We finally considered both STA and TTA processes as simultaneously contributing to exciton quenching by using the full model described in Equations (3) and (4) (Figure 3d). This complete model is able to fit the kinetic decay across the entire measured time range and at all excitation powers (see Figure S3 for corresponding data and fits for the additionally measured excitation densities of 4 and 20 mW cm⁻², Supporting Information).

While our STA+TTA model fits the measured PL decay completely, other loss processes could also be contributing to the

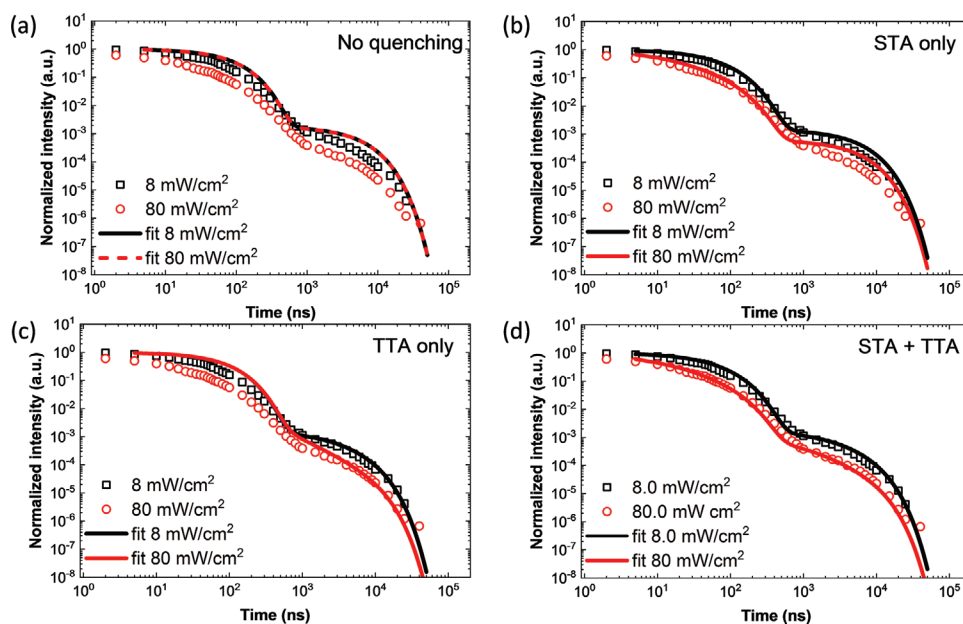


Figure 3. Normalized PL intensity versus time for a) no quenching processes, b) only STA, c) only TTA, and d) complete. Open symbols represent the measured data, whereas the lines correspond to a fit with our kinetic model.

PL decay dynamics. For example, singlet–singlet annihilation (SSA) is another process that could potentially reduce the singlet population. Figure S4 (Supporting Information) shows the influence of SSA on the power dependence of the PL transients. It does not reproduce the line shape of the experimental data as the fit gets steeper in the intermediate region compared to STA, nor can it be used in combination with another quenching process to obtain a good fit. This leads us to conclude that SSA is not a major decay process for singlet excitons, in agreement with previous findings.^[18] Furthermore, other recent work has proposed spontaneous dissociation of charge-transfer excitons as an additional exciton annihilation process.^[32] This, however, is most likely to occur in a fluorophore with a large permanent dipole moment, which would facilitate the process. CzDBA is a symmetric molecule, with dipole moment close to 0.^[33] We also carried out our measurements on films without any electrodes, precluding the possibility of an internal electric field which could influence spontaneous exciton dissociation.

From the kinetic modeling, we obtain a singlet lifetime of 98 ns which is in close agreement with the lifetime obtained in solution (Figure 2a). This validates that our modeling approach can accurately give the intrinsic singlet lifetime. The model successfully fits the PL decay transients at different power densities using a single set of power-independent rate constants of k_{ISC} , k_{rISC} , k_{TTA} , and k_{STA} (Table 1). This point is further illustrated in-depth in Figure S5 (Supporting Information), where

the two decays at 8 and 80 mW cm⁻² are fit using only STA in conjunction to changing k_{ISC} and k_{rISC} at every excitation power density. Although this method can also achieve a satisfactory fit for every excitation power, it requires a power dependent k_{rISC} , which is physically not realistic. Using this fitting approach for higher excitation powers, the lack of triplets normally disappearing by TTA has to be compensated in such a way that the value of k_{rISC} almost equals k_{rISC} , which for a down- and the up-hill process is physically not meaningful. An alternative explanation for an apparent power dependence of $r(\text{ISC})$ could originate from the presence of triplet-to-singlet FRET mechanisms.^[34] However, the possibility of this process diminishes with high rISC rate, as observed for CzDBA, which also contributes to the nearly 100% PLQY of CzDBA. Therefore, we do not expect triplet-to-singlet FRET to play a significant role in CzDBA photophysics.

Using the obtained quenching rate constants of $k_{\text{TTA}} = 8 \times 10^{-18} \text{ m}^3 \text{ s}^{-1}$ and $k_{\text{STA}} = 2.5 \times 10^{-17} \text{ m}^3 \text{ s}^{-1}$, we can also further evaluate the forward and reverse ISC rate constants k_{ISC} and k_{rISC} , which amount to 1.0×10^6 and $2.2 \times 10^5 \text{ s}^{-1}$, respectively (Table 1). We observe that the approximation of a biexponential decay leads to an overestimation of the k_{ISC} and k_{rISC} by more than an order of magnitude. A similar large value of k_{ISC} of $3.8 \times 10^7 \text{ s}^{-1}$ was reported in an earlier photophysical study on CzDBA using a three-exponential fit. However, the excitation density at which these data were taken was not provided.^[17]

Table 1. Values of several photophysical parameters for the biexponential model from the literature and our kinetic fits presented in Figure 3. *For the intrinsic triplet lifetime we assume a lower limit of 100 μs , such that phosphorescence does not play a role.

Method	τ_s [ns]	τ_t [μs]	k_{ISC} [s^{-1}]	k_{rISC} [s^{-1}]	k_{STA} [$\text{m}^3 \text{ s}^{-1}$]	k_{TTA} [$\text{m}^3 \text{ s}^{-1}$]
Biexponential fit ^[17]	34	1.0	1.7×10^7	6.7×10^5	–	–
Kinetic fit (this work)	98	100*	1.0×10^6	2.2×10^5	2.5×10^{-17}	8.0×10^{-18}

Comparison with our data suggests that these reported PL decays were taken at an elevated excitation density of around 80 mW cm^{-2} , as their PF lifetime of 34 ns corresponds well to our 33 ns from a biexponential fit at said power density. This shows that ignoring the effect of exciton quenching processes at too high excitation densities can give rise to large errors in the derived forward and reverse ISC rates.

We note that for the intrinsic triplet lifetime we used $100 \mu\text{s}$ as a lower limit. Since the rISC process is in the $3 \mu\text{s}$ regime this means that the triplet states are almost completely depopulated by this process only. Increasing the intrinsic triplet lifetime to 1 ms in our model does therefore not change the obtained forward and reverse ISC rates and quenching rates.

Furthermore, the k_{TTA} value obtained from the kinetic modeling and power dependent PL measurements ($k_{\text{TTA}} = 8 \times 10^{-18} \text{ m}^3 \text{ s}^{-1}$) is in very good agreement with a previous report, where k_{TTA} was extracted from the electrical efficiency roll off of a single layer CzDBA OLED, using a similar rate equation approach, where $k_{\text{TTA}} = 1 \times 10^{-17} \text{ m}^3 \text{ s}^{-1}$ was found.^[20] Here, TTA was found to be the dominant mechanism controlling the EQE roll-off^[20] without the need to include STA. However, in PL we have to take into account the occurrence of STA as well. This is likely connected to the difference in exciton generation mechanism. In an OLED, singlets and triplets are generated in a 1:3 ratio, assuming simple spin statistics. This is in stark contrast to the situation in PL, where only singlets are initially generated. We can qualitatively say that the difference in population implies a prevalence of TTA over STA in OLEDs, whereas this does not have to hold in PL.

The obtained rate constants allow us to visualize the impact of the STA and TTA processes on the triplet exciton population in PL. In **Figure 4**, the simulated triplet density versus time is displayed, including the two annihilation processes and, for comparison, also the situation of no quenching. For all three cases the triplet population exhibits a build-up via ISC until reaching a time τ_s (98 ns), after which rISC (and TTA if taken into account) causes it to decay. Taking STA into account leads to a reduction in the triplet density already at times below

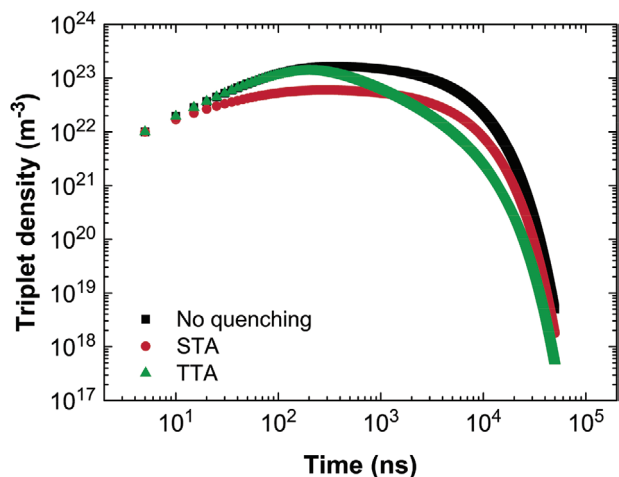


Figure 4. Triplet exciton density versus time. The triplet density is simulated with an initial singlet exciton density of $2 \times 10^{24} \text{ m}^{-3}$, corresponding approximately to a power density of 80 mW cm^{-2} .

100 ns, whereas the triplet density with TTA closely follows the situation of no quenching at early times. As already observed (Figure 3b), STA reduces the singlet population at early times, but through ISC it indirectly decreases the triplet population as well. The quadratic scaling of TTA with the triplet density means that it has almost no influence at these timescales. However, the negative impact of TTA is clearly seen at times beyond 100 ns, where after $\approx 1000 \text{ ns}$ the curve with TTA drops below the curve with STA. In the delayed fluorescence region ($> \approx 1000 \text{ ns}$) emissive singlets are generated from triplets through rISC and Figure 4 shows that the main quenching in this region originates from TTA.

We note that in practice TADF emitters are often diluted in a wide bandgap host, and in such a blend the contribution of the bimolecular annihilation processes will be weakened. Our above results focused on neat films because CzDBA in particular can attain high OLED performance even without a host.^[25] Nonetheless, we also measured the fluorescence decay dynamics in a host:guest sample (CBP: 10% CzDBA) and find that the power dependence disappears, as expected (Figure S6, Supporting Information). This confirms that the power dependence in the pristine films originates from bimolecular annihilation processes.

3. Conclusion

We have shown that the TRPL of TADF emitters can be strongly affected by the chosen excitation power due to various exciton quenching mechanisms, in particular STA and TTA. Application of biexponential or multiexponential decay models may lead to overestimation of the forward and reverse ISC rates. The kinetic modeling used in this study can accurately fit the TRPL spectra at various excitation powers and is capable of the direct determination of the intrinsic singlet lifetime, rate of (reverse) intersystem crossing, singlet–triplet annihilation and triplet–triplet annihilation constants. The obtained k_{TTA} value of $8 \times 10^{-18} \text{ m}^3 \text{ s}^{-1}$ is close to a previously obtained value from OLED data. Reliable characterization of PL decays aids in the development and evaluation of high-performance TADF materials.

4. Experimental Section

Sample Preparation: CzDBA was obtained from Luminescence Technology Corporation and CBP from Sigma-Aldrich. Both were used without further purification. Samples were prepared by evaporating 100 nm onto a quartz substrate under a base pressure of around $2 \times 10^{-6} \text{ mbar}$. The sample was loaded into a home-built air-tight sample holder inside a glovebox before it was transferred out for the spectroscopic measurements. All measurements were carried out at room temperature. A $5 \times 10^{-6} \text{ M}$ degassed solution of CzDBA in toluene was used for steady-state absorption and fluorescence, as well as for time-resolved fluorescence in solution. These measurements were done in a 2 mm path length quartz cuvette.

Spectroscopic Characterization: Steady-state absorption was measured on a home-built setup consisting of a deuterium halogen lamp (DH2000-DUV, OceanOptics) connected to a USB spectrometer (34000-UV-VIS-EIS, OceanOptics). Steady-state fluorescence was measured on a Horiba/Jobin Yvon Fluorolog-3 Spectrofluorometer,

using 400 nm excitation. TRPL measurements were carried out using a 4Picos gated-iCCD camera (Stanford Computer Optics). Samples were photoexcited at 350 nm using the output from a Ti: sapphire laser (Coherent, Astrella, 1 kHz, 5 mJ, 35 fs) paired with a commercial optical parametric amplifier (Coherent, OperA). The spectra are collected using the 4Spec software (Stanford Computer Optics) using gating times ranging exponentially from 0.5 to 5000 ns and spectra were recorded out to 50 μ s. The photoexcitation light was focused onto the sample in order to ensure a uniform excitation density throughout the film. The spot size of 0.8 mm at the sample position was characterized using a beam profiler (Coherent, LaserCamHR-II).

For the power study, the lowest incident power was chosen to minimize annihilation processes while maintaining a good signal-to-noise ratio. The power was varied at least an order of magnitude but kept the highest power low enough that bleaching or other degradation effects of the films during the measurement would play a minor role and would not impede the analysis.

Analysis: The initial singlet density was calculated from the absorption spectrum and the incident laser power using a reported method.^[23] At a low power density, where annihilation does not play a large role, the values of $k_{ISC}/k_{rISC}/\tau_s$ can be determined. The power dependence provides information on the various quenching processes, as detailed in the results and discussion section.

Quantum Chemical Calculations: To obtain reliable predictions of solid-state excited-state energy, the cost-effective ω -tuning protocol with PCM implicit solvent model ($\epsilon = 3.0$) is followed.^[35,36] The optimal ω can be obtained by introducing the target function (J) to be minimized, defined as

$$J(\omega) = |E_N(\omega) + \epsilon_{N,HOMO}(\omega) + |E_A(\omega) + \epsilon_{A,HOMO}(\omega)| \quad (5)$$

where the capital N and A stands for the neutral and anionic states, respectively. The computations were performed at ω B97X-D/def2-TZVP level of theory. The optimal ω for each compound was stored in the database, ranging from 0.010 to 0.040 Bohr⁻¹.

For the description of excited states, linear-response time-dependent density functional theory with Tamm–Dancoff approximation (TDA/TD-DFT) along with ω B97X-D*/def2-TZVP (with the optimal ω) is employed to compute the excitation energies and oscillator strengths.

Supporting Information

Supporting Information is available from the Wiley Online Library or from the author.

Acknowledgements

The authors would like to thank Kun-Han Lin for performing the quantum chemical calculations of the excited state energy levels.

Open access funding enabled and organized by Projekt DEAL.

Conflict of Interest

The authors declare no conflict of interest.

Data Availability Statement

The data that support the findings of this study are available from the corresponding author upon reasonable request.

Keywords

organic light-emitting diodes, transient photoluminescence, thermally activated delayed fluorescence

Received: August 25, 2021

Revised: October 26, 2021

Published online: December 6, 2021

- [1] J. Gibson, A. P. Monkman, T. J. Penfold, *ChemPhysChem* **2016**, *17*, 2956.
- [2] H. Uoyama, K. Goushi, K. Shizu, H. Nomura, C. Adachi, *Nature* **2012**, *492*, 234.
- [3] Y. Liu, C. Li, Z. Ren, S. Yan, M. R. Bryce, *Nat. Rev. Mater.* **2018**, *3*, 18020.
- [4] X. Xiong, F. Song, J. Wang, Y. Zhang, Y. Xue, L. Sun, N. Jiang, P. Gao, L. Tian, X. Peng, *J. Am. Chem. Soc.* **2014**, *136*, 9590.
- [5] K. Hanaoka, K. Kikuchi, S. Kobayashi, T. Nagano, *J. Am. Chem. Soc.* **2007**, *129*, 13502.
- [6] O. Franco, M. Jakoby, R. V. Schneider, F. Hundemer, D. Hahn, B. S. Richards, S. Bräse, M. A. R. R. Meier, U. Lemmer, I. A. Howard, *Front. Chem.* **2020**, *8*, 126.
- [7] H. Nakanotani, Y. Tsuchiya, C. Adachi, *Chem. Lett.* **2021**, *50*, 938.
- [8] F. B. Dias, K. N. Bourdakos, V. Jankus, K. C. Moss, K. T. Kamtekar, V. Bhalla, J. Santos, M. R. Bryce, A. P. Monkman, *Adv. Mater.* **2013**, *25*, 3707.
- [9] H. Noda, X. K. Chen, H. Nakanotani, T. Hosokai, M. Miyajima, N. Notsuka, Y. Kashima, J. L. Brédas, C. Adachi, *Nat. Mater.* **2019**, *18*, 1084.
- [10] L. G. Franca, Y. Long, C. Li, A. Danos, A. P. Monkman, *J. Phys. Chem. Lett.* **2021**, *12*, 1490.
- [11] C. Baleizão, M. N. Berberan-Santos, *J. Chem. Phys.* **2007**, *126*, 204510.
- [12] B. Yurash, H. Nakanotani, Y. Olivier, D. Beljonne, C. Adachi, T.-Q. Nguyen, *Adv. Mater.* **2019**, *31*, 1804490.
- [13] T. Serevičius, R. Skaisgiris, G. Kreiza, J. Dodonova, K. Kazlauskas, E. Orentas, S. Tumkevičius, S. Juršėnas, *J. Phys. Chem. A* **2021**, *125*, 1637.
- [14] O. V. Mikhnenko, P. W. M. Blom, T. Q. Nguyen, *Energy Environ. Sci.* **2015**, *8*, 1867.
- [15] I. Röhrich, Q. Niu, B. van der Zee, E. del Pino Rosendo, N. I. Crčićun, C. Ramanan, P. W. M. Blom, *Adv. Electron. Mater.* **2020**, *6*, 1700643.
- [16] K. Stavrou, L. G. Franca, A. P. Monkman, *ACS Appl. Electron. Mater.* **2020**, *2*, 2868.
- [17] T. L. Wu, M. J. Huang, C. C. Lin, P. Y. Huang, T. Y. Chou, R. W. Chen-Cheng, H. W. Lin, R. S. Liu, C. H. Cheng, *Nat. Photonics* **2018**, *12*, 235.
- [18] K. Masui, H. Nakanotani, C. Adachi, *Org. Electron.* **2013**, *14*, 2721.
- [19] A. Niwa, T. Kobayashi, T. Nagase, K. Goushi, C. Adachi, H. Naito, *Appl. Phys. Lett.* **2014**, *104*, 213303.
- [20] B. van der Zee, Y. Li, G.-J. A. H. Wetzelaer, P. W. M. M. Blom, *Adv. Opt. Mater.* **2021**, *9*, 2100249.
- [21] A. S. D. Sandanayaka, K. Yoshida, T. Matsushima, C. Adachi, *J. Phys. Chem. C* **2015**, *119*, 7631.
- [22] N. Haase, A. Danos, C. Pflumm, A. Morherr, P. Stachelek, A. Mekic, W. Brütting, A. P. Monkman, *J. Phys. Chem. C* **2018**, *122*, 29173.
- [23] M. Hasan, A. Shukla, V. Ahmad, J. Sobus, F. Bencheikh, S. K. M. McGregor, M. Mamada, C. Adachi, S.-C. C. Lo, E. B. Namdas, *Adv. Funct. Mater.* **2020**, *30*, 2000580.
- [24] T. Kobayashi, A. Niwa, K. Takaki, S. Haseyama, T. Nagase, K. Goushi, C. Adachi, H. Naito, *Phys. Rev. Appl.* **2017**, *7*, 034002.
- [25] N. B. Kotadiya, P. W. M. Blom, G.-J. A. H. Wetzelaer, *Nat. Photonics* **2019**, *13*, 765.

- [26] S. Thomson, *Edinburgh Instruments*, May 2019.
- [27] M. Lehnhardt, T. Riedl, T. Rabe, W. Kowalsky, *Org. Electron.* **2011**, *12*, 486.
- [28] H. D. Burrows, J. Seixas de Melo, C. Serpa, L. G. Arnaut, M. da G. Miguel, A. P. Monkman, I. Hamblett, S. Navaratnam, *Chem. Phys.* **2002**, *285*, 3.
- [29] S. J. Woo, Y. H. Ha, Y. H. Kim, J. J. Kim, *J. Mater. Chem. C* **2020**, *8*, 12075.
- [30] M. K. Etherington, J. Gibson, H. F. Higginbotham, T. J. Penfold, A. P. Monkman, *Nat. Commun.* **2016**, *7*, 13680.
- [31] F. B. Dias, T. J. Penfold, A. P. Monkman, *Methods Appl. Fluoresc.* **2017**, *5*, 012001.
- [32] T. Yamanaka, H. Nakanotani, C. Adachi, *Nat. Commun.* **2019**, *10*, 5748.
- [33] W. Liu, N. Kotadiya, P. W. M. Blom, G.-J. A. H. Wetzelaer, D. Adrienko, *Adv. Mater. Technol.* **2021**, *6*, 2000120.
- [34] L. E. de Sousa, L. dos Santos Born, P. H. de Oliveira Neto, P. de Silva, *ChemRxiv* **2021**, preprint <https://doi.org/10.33774/chemrxiv-2021-9b9p2>.
- [35] H. Sun, S. Ryno, C. Zhong, M. K. Ravva, Z. Sun, T. Körzdörfer, J. L. Brédas, *J. Chem. Theory Comput.* **2016**, *12*, 2906.
- [36] H. Sun, Z. Hu, C. Zhong, X. Chen, Z. Sun, J. L. Brédas, *J. Phys. Chem. Lett.* **2017**, *8*, 2393.